Chinese Chemical Letters 35 (2024) 108674

Contents lists available at ScienceDirect

Chinese Chemical Letters

journal homepage: www.elsevier.com/locate/cclet

$CoFe_2O_4$ decorated graphene/C_{18}-functionalized mesoporous silica nanocomposites prepared for magnetic enrichment and electrochemical detection of promethazine in beef

Xingdong Yang[a], Shi-Ming Ying[a], Sen Zhang[a], Jinxia Dai[a], Wei Gao[a], Tian-Qi Wang[a], Jun-Qin Qiao[a], Hong-Zhen Lian[a,*], Li Mao[b,*]

[a] State Key Laboratory of Analytical Chemistry for Life Science, School of Chemistry & Chemical Engineering and Centre of Materials Analysis, Nanjing University, Nanjing 210023, China
[b] Ministry of Education (MOE) Key Laboratory of Modern Toxicology, School of Public Health, Nanjing Medical University, Nanjing 211166, China

ARTICLE INFO

Article history:
Received 16 February 2023
Revised 15 May 2023
Accepted 8 June 2023
Available online 10 June 2023

Keywords:
Promethazine (PHZ)
Drug residue
Magnetic solid phase extraction
Electrochemical detection
Beef

ABSTRACT

Promethazine (PHZ) is used as a sedative in veterinary medicine, and its residue can threaten the health of human. The electrochemical detection of PHZ is suitable method for application in the field. However, the traditional electroanalysis is difficult to perform directly in meat samples due to matrix interference. This work integrates magnetic solid-phase extraction and differential pulse voltammetry for highly sensitive and selective determination of PHZ in beef and beef liver for the first time. $CoFe_2O_4$/graphene coated with C_{18}-functionalized mesoporous silica (MG@mSiO_2-C_{18}) is synthesized as dispersed magnetic adsorbent to extract PHZ. Magnetic glassy carbon electrode modified with nitrogen-doped hollow carbon microspheres (HCM) attracts the MG@mSiO_2-C_{18} with PHZ, and directly detects the PHZ without elution procedure. MG@mSiO_2-C_{18} can separate PHZ to avoid the interference of impurities on following detection, and also concentrate PHZ on magnetic electrode. Additionally, the electrode modification with HCM can amplify the electrochemical signal of PHZ. Finally, the integrated PHZ determination method exhibits a wide linear range from 0.08 μmol/L to 300 μmol/L with a low limit of detection of 9.8 nmol/L. The beef sample analysis presents excellent recovery, demonstrating that this protocol is promising for the rapid and onsite detection of PHZ in real meat samples

Promethazine (PHZ), a kind of phenothiazine antihistamines, is a sedative with central nervous system depression. It is commonly used to prevent and cure nausea and emesis caused by motion sickness and surgery [1], and treat psychotic disorders such as schizophrenia, mania and depression [2]. In animal medicine, PHZ is frequently used as veterinary drug to decrease the activity for growth promotion and fattening during feeding, and reduce weight loss and mortality during the transportation of animals [3]. The residue of PHZ in animal-derived food can contribute the serious harm on human body, such as coma, neurologic abnormality, extrapyramidal effect, respiratory depressions and even death [4]. The European Union has early prohibited the use of the phenothiazines [5], and in 2011, the Ministry of Agriculture of the People's Republic of China issued an announcement prohibiting the use of PHZ in animal feed and drinking water [6]. As a consequence, it is extremely important to develop reliable and applicable methods for determination of PHZ in animal-derived food, the main source of proteins for humans.

The chromatography coupled with different detection systems is the most universal technique for analysis of the residues of veterinary drugs in animal-derived food because of its high reliability and wide acceptance [7,8]. In the U.S. Food and Drug Administration (FDA) Foods Program Compendium of Analytical Methods, liquid chromatography tandem mass spectrometry (LC-MS) is used by FDA regulatory laboratories for the determination of psychotropic drugs in ingredients of animal origin [9]. Coincidentally, the LC-MS is employed for the determination of PHZ in meat in the standard method promulgated by the Chinese government departments. The chromatographic separation is carried out on a C_{18} column, in which a mixture of formic acid solution-acetonitrile is used as the mobile phase. The mass spectrometry with an electrospray ionization source is performed to detect PHZ [6]. However, the sophisticated instrumentation, well-trained personnel and a relative long analysis time are required in LC-MS analysis, which limits the deployment of it in onsite, rapid and real time applica-

* Corresponding authors.
E-mail addresses: hzlian@nju.edu.cn (H.-Z. Lian), maoli@njmu.edu.cn (L. Mao).

https://doi.org/10.1016/j.cclet.2023.108674
1001-8417/

tions. It should be noted that the matrix complexity of meat samples and low concentrations of the existing drugs generally require laborious and time-consuming procedures of samples pretreatment and target enrichment before chromatography-based assays. The solid-phase extraction (SPE) is one of the most frequently used techniques in samples pretreatment due to its facile preparation, low cost, low solvent consumption and high extraction efficiency [10]. SPE techniques based on various functionalized materials are usually used in combination with chromatographic analysis for the determination of PHZ in meat samples [11,12]. However, it generally has multistep separation operations and adsorbent loss shortcomings. As a contrast with traditional SPE, the SPE based on dispersive magnetic materials that is called magnetic solid-phase extraction (MSPE) can rely on an external magnetic field even a magnet to achieve the separation of solid adsorbent and matrix, which consequently improves the separation efficiency and simplifies the operation procedure [13,14]. Therefore, MSPE has been widely applied to the pretreatment of intricate environmental and biological samples in recent years [15,16]. At present, however, MSPE has rarely been applied to the pretreatment of meat samples for PHZ prior to chromatography-based methods.

The electrochemical method has been attracting extensive attention due to the high sensitivity, rapid response, operational simplicity and low cost [17,18]. Recently, some efforts have been going on to develop advanced electrode modification materials for the response signal amplification in electrochemical detection of PHZ [19,20]. Despite the desired sensitivity and selectivity have been achieved, the complex matrix such as the animal-derived food is apt to make the electrochemical methods difficult to perform satisfactorily, which forces the samples pretreatment techniques to be equipped prior to the detection. To our best knowledge, however, there have been no reports yet that SPE technology including MSPE was introduced to the pretreatment of meat sample for PHZ detection before electrochemical methods. On the other hand, magnetic separation is a facile pretreatment technique for electrochemical methods to reach the requirement of rapid and onsite detection. Target analytes are normally determined through different electrochemical methods after desorbed from magnetic absorbents by small volume eluent [21,22]. Because magnetic electrode can attract the magnetic materials absorbing target analytes dispersed in the sample solution, sometimes, the direct detection of target analytes is achieved on the electrode without the elution procedure [23,24]. Therefore, we integrated the MSPE separation technique and the electrochemical detection method based on magnetic electrodes for facile and quick separation and determination of PHZ in beef or beef liver samples.

Herein, we prepared magnetic graphene (MG) firstly, and then wrapped the MG by C_{18} groups functionalized mesoporous silica (MG@mSiO_2-C_{18}) to capture PHZ (Scheme 1A). The $CoFe_2O_4$ nanoparticles have more surface hydroxyl (M-OH) species than Fe_3O_4 [25], and the cobalt tends to form coordination bond with amine groups more likely than iron [26]. As a result, $CoFe_2O_4$ replaced the classical Fe_3O_4 as the magnetic core. Moreover, the vertical coating of organic-inorganic hybrid mesoporous silica on the MG composites could improve the interfacial properties of graphene and provide aligned mesoporous structure [27,28]. The modification with hybrid C_{18}-mesoporous silica allows the prepared material to possess not only unique hydrophobic sites but also mechanical, thermal and chemical stabilities [29,30]. The MG@mSiO_2-C_{18} is expected to be an ideal MSPE absorbent for PHZ enrichment based on the strong hydrophobic interaction of PHZ ($\log K_{ow}$ 4.81) with C_{18} groups, the coordination of amine groups in PHZ with cobalt as well as iron in $CoFe_2O_4$, and the π-π stacking interaction of benzene rings in PHZ and graphene. On the other hand, the magnetic electrode was modified with nitrogen-doped hollow carbon microspheres (HCM) with enhanced catalytic activity and excellent electrical conductivity [31,32]. The PHZ loaded magnetic adsorbents in solution were gathered onto the surface of magnetic electrode, further increasing the detection sensitivity toward the target analytes without the conventional solvent elution step in general MSPE operation (Scheme 1B). After systematical methodology verification, the proposed integrated approach of MSPE pretreatment and electrochemical detection was practically applied to the determination of PHZ residue in beef and beef liver samples.

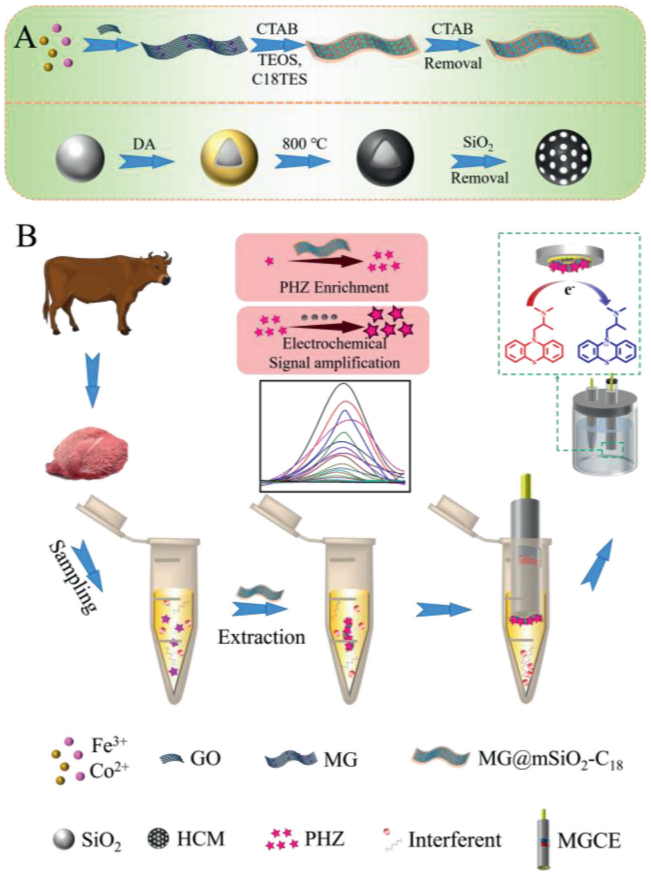

Scheme 1. (A) The preparation process of the MG@mSiO_2-C_{18} nanocomposites and HCM microspheres. (B) The schematic illustration of MSPE enrichment and electrochemical detection of PHZ.

As shown in Scheme 1A, the magnetic $CoFe_2O_4$ particles were decorated onto graphene oxide (GO) *via* a solvothermal reaction. The MG was encapsulated by C_{18}-functionalized hybrid mesoporous silica using a facile sol-gel synthesis method.

The morphologies and sizes of MG and MG@mSiO_2-C_{18} were observed using transmission electron microscopy (TEM). Fig. 1A represents a typical TEM image of graphene with wrinkles, and the ~150 nm $CoFe_2O_4$ nanoparticles are anchored onto graphene sheet. The involvement of nanoparticles would prevent the restacking of graphene sheets after GO was reduced under the hydrothermal condition. In MG@mSiO_2-C_{18} TEM images (Figs. 1B and C), the translucent layer with a thickness of about 50 nm could be seen, suggesting that the C_{18}-functionalized mesoporous silica was coated on the whole MG.

The FT-IR spectra were used to inspect the nanocomposites construction and the surface functional groups. As shown in Fig. 1D, the broad band at around 3420 cm^{-1} and the peaks of 1724 and 1625 cm^{-1} in GO curve are attributed to the vibrations of O–H and C=C, respectively. The MG curve, comparing with the GO curve, has a newly formed peak at 579 cm^{-1} produced by Fe–O–Fe/Co–O–Co vibration in $CoFe_2O_4$ nanoparticles, which ver-

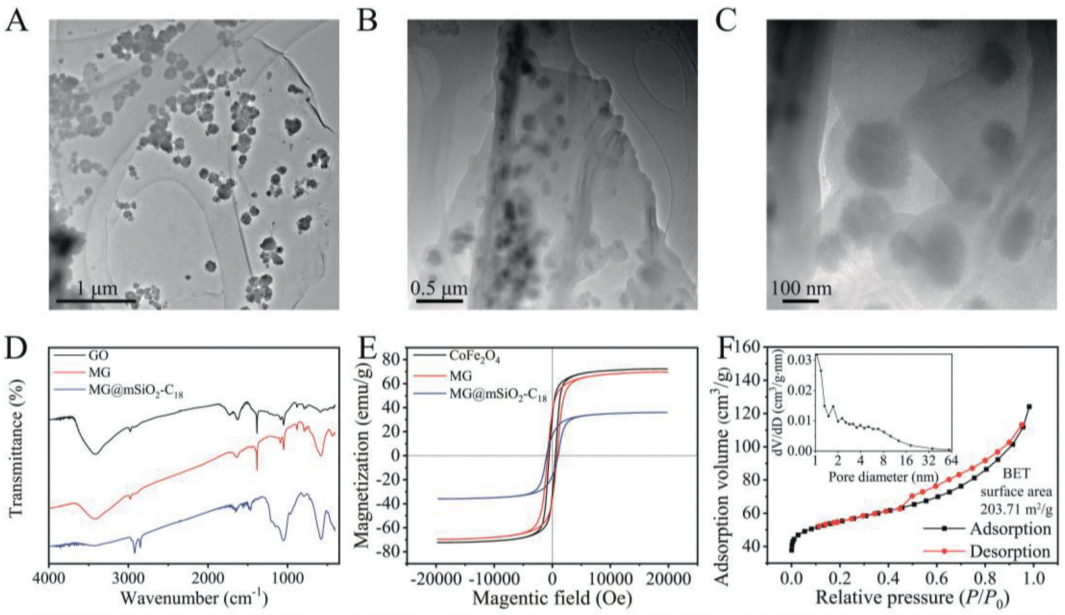

Fig. 1. TEM of (A) MG and (B, C) MG@mSiO$_2$-C$_{18}$ nanocomposites. (D) FT-IR spectra of GO, MG and MG@mSiO$_2$-C$_{18}$. (E) Magnetization curves of $CoFe_2O_4$, MG and MG@mSiO$_2$-C$_{18}$. (F) N_2 adsorption-desorption isotherms of MG@mSiO$_2$-C$_{18}$. Inset: Pore size distribution of MG@mSiO$_2$-C$_{18}$.

ifies the nanoparticles anchored to graphene. In the MG@mSiO$_2$-C$_{18}$ curve, two emerging peaks at 2920 and 2850 cm^{-1} are attributed to the vibration of $-CH_2-$ in C$_{18}$ groups, two faint peaks at 2956 and 2871 cm^{-1} to $-CH_3$, and those at 1259 and 1050 cm^{-1} (broad peak) to the vibration of Si–C and Si–O–Si respectively in the organic-inorganic hybrid mesoporous silica. All of the FT-IR spectra suggested the successful synthesis of MG@mSiO$_2$-C$_{18}$.

Fig. 1E shows the magnetic hysteresis loops to assess the magnetic behavior of the prepared nanocomposites. The wide hysteresis presented from $CoFe_2O_4$, MG and MG@mSiO$_2$-C$_{18}$ is typical characteristic of the hard magnetic behavior of $CoFe_2O_4$. Moreover, the $CoFe_2O_4$, MG and MG@mSiO$_2$-C$_{18}$ possess the specific saturation magnetization of 72.4, 69.4, 36.0 emu/g, respectively. Although the magnetism of MG@mSiO$_2$-C$_{18}$ decreased in comparison with $CoFe_2O_4$ and MG due to the encapsulation of mesoporous silica, the saturation magnetization still makes the nanocomposites sufficiently easy to separate from solution in an external magnetic field.

The N_2 adsorption-desorption isotherms of MG and MG@mSiO$_2$-C$_{18}$ are shown in Fig. S2 (Supporting information) and Fig. 1F, respectively, and the latter shows the representative IV type curve with a sharp capillary condensation step at a relative pressure of approximately 0.5. The Brunauer-Emmett-Teller (BET) surface area of MG@mSiO$_2$-C$_{18}$ is 203.71 m^2/g, which is much larger than that of MG of 22.22 m^2/g. Besides, the most common Barrett-Joyner-Halenda (BJH) model was employed to calculate the MG@mSiO$_2$-C$_{18}$ with average pore size of 4.62 nm, and the pore size distribution is also shown in Fig. 1F (inset). The mesoporous structure of MG@mSiO$_2$-C$_{18}$ coming from the organic-inorganic hybrid silica could promote the exposure of more functional groups for improving the adsorption activity, which profits from the rigid network skeleton [33].

The crystal structure and the disorder of graphene in MG@mSiO$_2$-C$_{18}$ nanocomposites were studied by the X-ray diffractomer (XRD) and Raman spectra. Additionally, the morphology, elements distribution and phase composition of MG@mSiO$_2$-C$_{18}$ were explored by TEM with energy dispersive X-ray spectrometry (EDS) and X-ray photoelectron spectroscopy (XPS). The analytical results of XRD, Raman spectra, TEM, EDS and XPS are supplied in Figs. S3-S7 in Supporting information, which further supports the successful construction of MG@mSiO$_2$-C$_{18}$.

The electrode modification material, HCM, was synthesized as shown in Scheme 1A. The morphologies and microstructures of HCM were characterized by TEM. In Fig. 2A, the resulting HCM displays a hollow spherical structure and ~330 nm uniform size. High-angle annular dark-field scanning TEM (HAADF-STEM) and N element EDS mapping analysis (Figs. 2B and C) indicate a homogeneous distribution of N element, proving the formation of N-doped HCM. The results of EDS spectrum reveals that the N content is about 6% in HCM. The XPS full-scan spectra and high-resolution spectra of C 1s and O 1s are shown in Fig. S9 (Supporting information), and no characteristic peak of Si indicates that the template SiO_2 is removed. The high-resolution N 1s spectrum (Fig. 2D) was used to characterize the type of N dopants which highly determines the performance of the electrocatalyst. The N 1s spectrum shows that N element mainly exists in the form of pyridinic N (~398.3 eV), pyrrolic N (~399.8 eV), graphitic N (~400.8 eV) and oxidized N (~402.3 eV), which reveals that the graphitic N of HCM has the highest relative ratio. The graphitic N can induce non-uniform electron distribution on adjacent carbon atoms and enhance the electrochemical catalytic activity [34].

The electrochemical properties of HCM modified electrode were investigated *via* cyclic voltammetry (CV) and electrochemical impedance spectroscopy (EIS) in 0.1 mol/L of KCl solution containing 5 mmol/L $[Fe(CN)_6]^{3-/4-}$. The typical CV responses and Nyquist plots of bare magnetic glassy carbon electrode (MGCE) and HCM/MGCE are shown in Figs. 2E and F, respectively. The CV anodic peak current of HCM/MGCE (184.7 μA) is about 2.5 times that of bare MGCE (74.1 μA), and the former displays a lower peak potential. The R_{ct} values for MGCE and HCM/MGCE in Nyquist plots were calculated as 1485 Ω and 26.59 Ω, respectively. These results of electrochemical measurement reveal that HCM is equipped with enhanced catalytic activity and excellent electrical conductivity, which should be ascribed to the synergistic effects of hollow structure and doping of N [35].

Fig. 3A shows UV–vis absorption spectra of 600 μmol/L PHZ before and after adsorption by MG, MG@mSiO$_2$ and MG@mSiO$_2$-C$_{18}$, respectively, by soaking 1 mg of adsorbent into PHZ aqueous solution. The PHZ absorbance of supernatant declined following the adding of above three adsorbents, which means the concentration of PHZ decreases. Among that, MG@mSiO$_2$-C$_{18}$ has the highest ef-

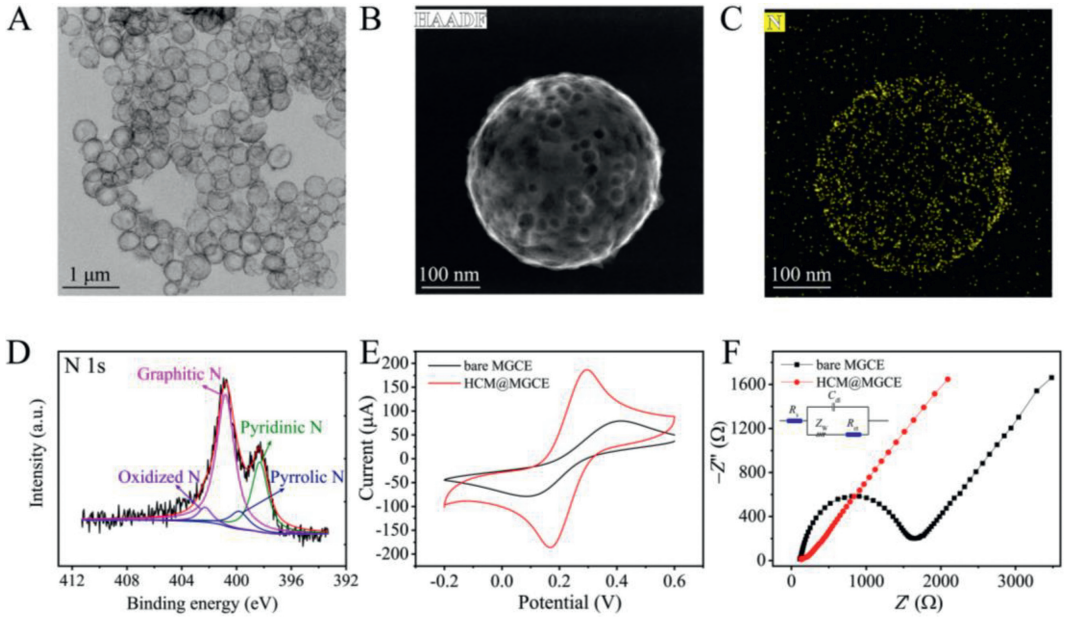

Fig. 2. TEM (A), HAADF-STEM image (B) and the corresponding EDS N elemental mapping images (C) of HCM. (D) XPS high-resolution N 1s spectrum of HCM. CV (E) and EIS (F) in 0.1 mol/L KCl solution containing 5 mmol/L (1:1) $[Fe(CN)_6]^{3-/4-}$ acquired at bare MGCE and HCM/MGCE.

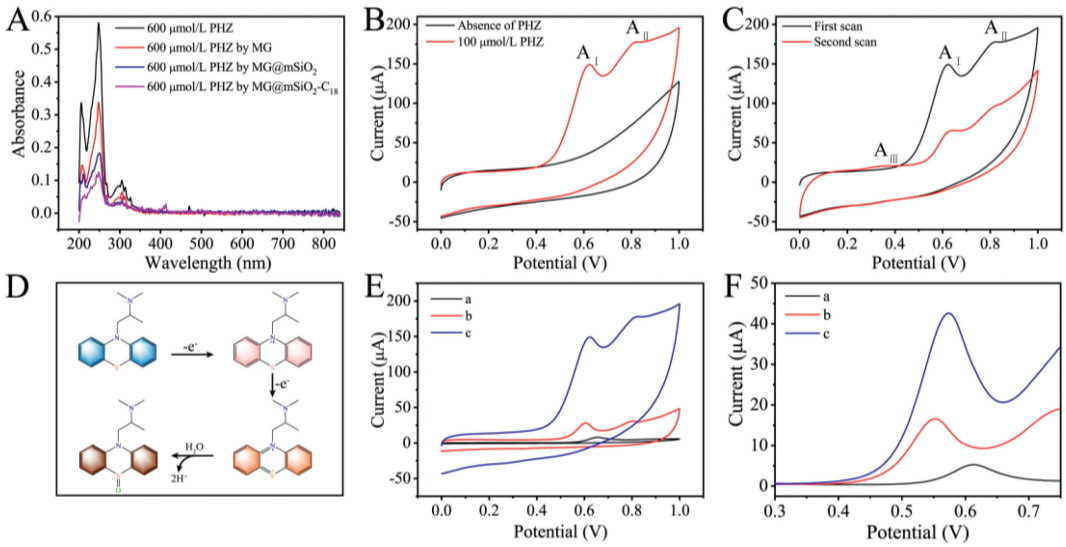

Fig. 3. (A) UV–vis absorption spectra of 600 μmol/L PHZ and the supernatant of 600 μmol/L PHZ after enriching by different nanocomposites. (B) CV recorded from HCM/MGCE after enriching by MG@mSiO$_2$-C$_{18}$ in absence and presence of PHZ. (C) The first and second CV scans recorded from HCM/MGCE after enriching by MG@mSiO$_2$-C$_{18}$ toward 100 μmol/L PHZ. (D) Electrooxidation mechanism of PHZ. CV (E) and DPV (F) recorded from different operating processes toward 100 μmol/L PHZ. a: MGCE without enrichment, b: HCM/MGCE without enrichment, and c: HCM/MGCE with enrichment by MG@mSiO$_2$-C$_{18}$. A: 0.1 mol/L PBS, pH 8.3; B-E: 0.1 mol/L PBS + 0.1 mol/L KCl, pH 6.0.

fect for PHZ adsorption, indicating that it can be used as the ideal MSPE material for PHZ enrichment.

The electrochemical behavior of PHZ adsorbed by MG@mSiO$_2$-C$_{18}$ on HCM/MGCE was investigated by CV and differential pulse voltammetry (DPV). No visible peak was observed in absence of PHZ, while two obvious anodic peaks at 0.63 V (A_I) and 0.82 V (A_{II}) were identified in presence of PHZ (Fig. 3B). Interestingly, an inconspicuous anodic peaks (A_{III}) appeared at 0.34 V only during the second scan (Fig. 3C). The electrooxidation mechanism of PHZ is illustrated in Fig. 3D. In the first scan, one electron was removed from N atom in phenothiazine molecular skeleton to yield a relatively stable cation radical, generating the A_I. And the A_{II} at higher potentials was inferred to attribute to the oxidation of the tertiary nitrogen in the lateral chain [36]. In the second scan, another electron was removed from S atom to yield a divalent cation that underwent hydrolysis to produce PHZ sulfoxide, generating A_{III} [37].

The anodic peak of PHZ in CV, acquired by immersing the HCM/MGCE directly into 100 μmol/L PHZ solution, presents enhanced peak current with a lower peak potential compared with that from bare MGCE, which reveals the enhanced catalytic activity and fast electron transfer of HCM/MGCE toward PHZ (Fig. 3E). After PHZ was enriched by MG@mSiO$_2$-C$_{18}$, the anodic peak of PHZ on HCM/MGCE presents tremendously increased peak current, indicating that the enrichment effect of MG@mSiO$_2$-C$_{18}$ can greatly enhance the current signal response of PHZ on HCM/MGCE. The DPV, a highly sensitive technique, was performed from 0.30 V to 0.75 V to investigate the peak A_I in presence of 100 μmol/L PHZ (Fig. 3F). The results are consistent with those of CV, which af-

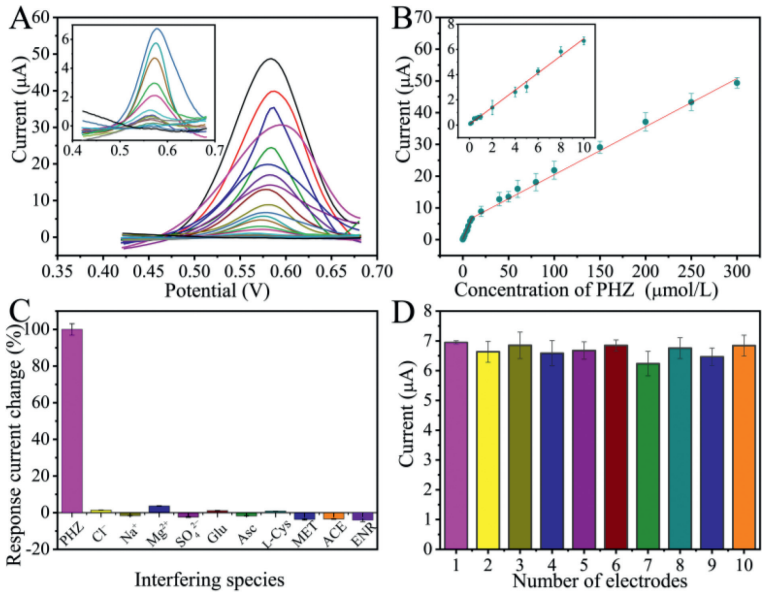

Fig. 4. (A) DPV responses at HCM/MGCE toward PHZ of different concentrations. (B) The linear relationship between the concentration of PHZ and current intensity at 0.57 V. (C) The effect of interfering species in electrochemical detection of PHZ at HCM/MGCE. (D) The reproducibility analysis on ten modified electrodes toward 10 μmol/L PHZ. Insets of A and B show Zoom in display of the DPV curves and calibration plot for low concentrations, respectively.

firms that HCM modification and MG@mSiO$_2$-C$_{18}$ enrichment toward PHZ can synergistically increase the sensitivity of PHZ detection in DPV.

It is concluded that the combination of MSPE and electrochemical detection is a strategy of killing three birds with one stone: firstly, the functionalized magnetic nanocomposites selectively capture and enrich the target analytes in sample solutions; secondly, the waiver of elution procedure saves the solvent consumption, and the analysis labor and time; and thirdly, the modification of magnetic electrode can enhance the electrochemical signals of analytes. Therefore, the protocol should offer a potential platform for the selective, sensitive and convenient detection of PHZ residues in animal-derived food.

Before assessing the effect of MSPE enrichment by MG@mSiO$_2$-C$_{18}$ and DPV detection based on HCM/MGCE toward PHZ, several relevant parameters were investigated (see Supporting information), in which the adsorption time was optimized to be 30 min, the pH of sample solution to be 8.3, the amount of MG@mSiO$_2$-C$_{18}$ to be 0.75 mg, and the pH of supporting electrolyte to be 6.0. Under the optimal experimental conditions, a series of PHZ solutions at different concentrations were detected electrochemically after enrichment by MG@mSiO$_2$-C$_{18}$. As shown in Fig. 4A, the peak current at 0.57 V in DPV gradually increased following the incremental PHZ concentration from 0.08 μmol/L to 300 μmol/L. The corresponding calibration plot exhibited good linearity between the peak value and PHZ concentration in two ranges of 0.08–10 μmol/L and 10–300 μmol/L (Fig. 4B). In lower PHZ concentration, the linear regression equation of I (μA) = 0.679 C_{PHZ} (μmol/L) + 0.052 with R^2 of 0.995 was acquired, and another equation of I (μA) = 0.151 C_{PHZ} (μmol/L) + 5.296 was acquired with R^2 of 0.997 in higher PHZ concentration. The limit of detection (LOD) was calculated to be 9.8 nmol/L based on the S/N = 3. To evaluate the protocol of PHZ electrochemical detection after enrichment by MG@mSiO$_2$-C$_{18}$-HCM/MGCE, the key analytical characteristics were tabulated in Table S1 (Supporting information) to compare with the previously literatures for the determination of PHZ. It is obvious that the considerable low LOD and broad linear range were obtained.

The interference study of as-proposed PHZ detection protocol was carried out at HCM/MGCE after enrichment by MG@mSiO$_2$-C$_{18}$ with different ions (Cl^-, Na^+, Mg^{2+} and SO_4^{2-}), several biological compounds (glucose (Glu), ascorbic acid (Asc) and L-cysteine (L-Cys)), and common veterinary drugs (metronidazole (MET), acetaminophen (ACE) and enrofloxacin (ENR). The interfering substances mentioned above at concentrations 10 times higher than PHZ were introduced individually to monitor the A_I peak current. As shown in Fig. 4C, the peak current signal at 0.57 V is not distinctly varied, which means that the developed method of PHZ detection was equipped with superior anti-interference capability.

The reproducibility as an important indicator of analysis accuracy was examined on different HCM/MGCE toward 10 μmol/L PHZ. It could be seen from Fig. 4D that the slight change of current responses as well as the low relative standard deviation (RSD) (3.2%) among 10 electrodes indicate the adequate reproducibility of the proposed PHZ detection protocol. In addition, the stability of MG@mSiO$_2$-C$_{18}$ for the enrichment and detection of PHZ was investigated. The current responses of PHZ did not exhibit apparent changes within a week. It still accounted for 96.5% of the original value on the ninth day (Fig. S14 in Supporting information), suggesting that the MG@mSiO$_2$-C$_{18}$ possesses satisfactory stability.

The determination method with satisfactory analytical performance was applied for PHZ detection in beef and beef liver samples. Firstly, different doses of PHZ were added into above sample minces, and then they were extracted by acidic acetonitrile. The MG@mSiO$_2$-C$_{18}$ was used to capture the target PHZ. Subsequently, the MG@mSiO$_2$-C$_{18}$ carrying PHZ was attracted by the magnetic HCM/MGCE, and then the PHZ was detected directly by DPV without an additional elution process. The analytical results are shown in Table 1, and the detected PHZ concentrations are approximate with the actually spiked doses. Additionally, the recoveries are all between 81.5% and 97.2% and the RSDs less than 4.5%, demonstrating that the as-proposed PHZ detection protocol has the promising potential for rapid and on-site PHZ detection in meat food.

In summary, a novel strategy for the determination of PHZ was developed based on MSPE enrichment with MG@mSiO$_2$-C$_{18}$ and electrochemical detection by DPV on HCM/MGCE. The MG@mSiO$_2$-C$_{18}$ with mesoporous structure captures the target PHZ *via* hy-

Table 1
Recovery experiments of PHZ in beef and beef liver samples on HCM/MGCE after enrichment by MG@mSiO_2-C_{18}.

Samples	Added (μmol/L)	Found (μmol/L)	Recovery (%)	RSD (%)
Beef	0	0		
	0.2	0.165	82.5	4.5
	1	0.922	92.2	3.2
	10	9.715	97.2	1.8
Beef	0	0		
liver	0.2	0.163	81.5	1.4
	1	0.913	91.3	1.2
	10	9.607	96.1	2.2

drophobic interaction of PHZ molecules with C_{18}, coordination of the amine groups with cobalt as well as iron, and π-π stacking interaction of benzene rings in PHZ and graphene, and the organic-inorganic hybrid endues the mesoporous silica with excellent structural stability. The HCM/MGCE can easily attract the MG@mSiO_2-C_{18} carrying PHZ magnetically without the elution process necessary in official standard method, and then the adsorbed PHZ can be on-electrode detected *via* DVP. Eventually, a broad linear range was achieved for PHZ detection with the remarkably low LOD. The real beef and beef liver samples fortified with PHZ were successfully analyzed with satisfactory reliability, which validates the practical application feasibility of the combination of MSPE and electroanalysis. The most interesting merit of this study is that, from the aspect of electrochemical method, DPV technique is effectively extended to the selective and sensitive determination of PHZ in meat samples after facile MSPE pretreatment by using MG@mSiO_2-C_{18} as the adsorbent. Another one is that, from the aspect of sample pretreatment, the traditional SPE procedure for LC-MS analysis of PHZ in the intricate matrices is greatly simplified when the electrochemical detection is introduced on the magnetic electrodes modified by nitrogen-doped HCM.

Declaration of competing interest

The authors declare that they have no known competing financial interests or personal relationships that could have appeared to influence the work reported in this paper.

Acknowledgments

This work was supported by the National Key R&D Program of China (No. 2019YFC1605400) and the National Natural Science Foundation of China (Nos. 21874065 and 22176085).

Supplementary materials

Supplementary material associated with this article can be found, in the online version, at doi:10.1016/j.cclet.2023.108674.

References

[1] A.L. Kovac, Drugs 59 (2000) 213–243.
[2] A.S. Horn, S.H. Snyder, Proc. Natl. Acad. Sci. U. S. A. 68 (1971) 2325–2328.
[3] B.L. Gao, J. Liu, L.X. Dong, et al., Anal. Biochem. 454 (2014) 7–13.
[4] K.S. Dyer, A.D. Woolf, Drug Saf. 21 (1999) 81–90.
[5] J. Cooper, P. Delahaut, T.L. Fodeya, C.T. Elliott, Analyst 129 (2004) 169–174.
[6] S. Wang, W. Guo, Y. Li, et al., Method of the Determination of Promethazine in Meat and Viscera of Livestock, Food Supplementary Test Method Database, State Administration for Market Regulation, BJS (2020) 202005 https://www.samr.gov.cn/spcjs/bcjyff/202011/P020201120634004572262.pdf.
[7] C.Y. Shen, D.X. Shen, T. Ding, et al., J. Liq. Chromatogr. Relat. Technol. 34 (2011) 1415–1430.
[8] Z. Yin, T. Chai, P. Mu, et al., J. Chromatogr. A 1463 (2016) 49–59.
[9] T.J. Nickel, C.R. Casey, https://www.fda.gov/media/120102/download, 2020.
[10] Z. Liu, J. Wang, Y. Guo, et al., J. Chromatogr. A 1678 (2022) 463345.
[11] T. Kumazawa, C. Hasegawa, S. Uchigasaki, et al., J. Chromatogr. A 1218 (2011) 2521–2527.
[12] J. Li, J. An, Y. Jiang, J. Chromatogr. A 1620 (2020) 461000.
[13] H.M. Jiang, Z.P. Yan, Y. Zhao, X. Hu, H.Z. Lian, Talanta 94 (2012) 251–256.
[14] Y. Li, X. Xu, H. Guo, et al., Anal. Chim. Acta 1219 (2022) 339984.
[15] J. Ashley, M.A. Shahbazi, K. Kant, et al., Biosens. Bioelectron. 91 (2017) 606–615.
[16] J.Y. Li, Z.M. Cao, Y. Hua, et al., Anal. Chem. 92 (2020) 1058–1067.
[17] W. Ruankham, T. Tantimongcolwat, K. Phopin, et al., Sensor. Actuator. B: Chem. 372 (2022) 132614.
[18] H. Gao, J. Yao, B. Jiang, R. Yuan, Y. Xiang, Sensor. Actuator. B: Chem. 371 (2022) 132530.
[19] K. Alagumalai, M. Balamurugan, S.M. Chen, M. Selvaganapathy, Microchem. J. 159 (2020) 105381.
[20] B. Thirumalraj, D.P. Jaihindh, S.O. Alaswad, et al., Environ. Res. 212 (2022) 113636.
[21] N. Ben Messaoud, A.A. Lahcen, C. Dridi, A. Amine, Sensor. Actuator. B: Chem. 276 (2018) 304–312.
[22] F. Long, J. Wang, Z. Zhang, L. Yan, J. Electroanal. Chem. 777 (2016) 58–66.
[23] X. Liu, F. Wang, Y. Meng, et al., Biosens. Bioelectron. 207 (2022) 114208.
[24] M. Sayhi, O. Ouerghi, K. Belgacem, et al., Biosens. Bioelectron. 107 (2018) 170–177.
[25] S. Zhang, H. Niu, Y. Cai, X. Zhao, Y. Shi, Chem. Eng. J. 158 (2010) 599–607.
[26] P.Y. Keng, B.Y. Kim, I.B. Shim, et al., ACS Nano 3 (2009) 3143–3157.
[27] J. Feng, X. She, X. He, et al., Food Chem. 239 (2018) 612–621.
[28] N. Sun, C. Deng, Y. Li, X. Zhang, ACS Appl. Mater. Interfaces 6 (2014) 11799–11804.
[29] M.L. Chen, M.M. Zheng, Y.Q. Feng, J. Chromatogr. A 1217 (2010) 3547–3556.
[30] Y. Hua, L.Y. Li, H. Min, et al., Microchem. J. 158 (2020) 105210.
[31] Y. Dong, L. Zhang, Sensor. Actuator. B: Chem. 368 (2022) 132140.
[32] R. Zhu, L. Li, Z. Wang, et al., ACS Nano 16 (2022) 1119–1133.
[33] J.J. Fei, X.H. Wu, Y.L. Sun, et al., Anal. Chim. Acta 1162 (2021) 338477.
[34] G. Wang, Y. Sun, D. Li, et al., Angew. Chem. Int. Ed. 54 (2015) 15191–15196.
[35] H. Yang, S. Li, H. Yu, et al., Nanoscale 11 (2019) 8950–8958.
[36] B. Blankert, H. Hayen, S.M. van Leeuwen, et al., Electroanalysis 17 (2005) 1501–1510.
[37] N. Sebastian, W.C. Yu, Y.C. Hu, D. Balram, Y.H. Yu, J. Alloy. Compd. 890 (2021) 161768.